CrossMark

Chlorinated styrene butadiene rubber/ zinc sulfide: novel nanocomposites with unique properties- structural, flame retardant, transport and dielectric properties

V. C. Jasna[1] · T. Anilkumar[1] · Adarsh A. Naik[2] · M. T. Ramesan[1]

Abstract

Chlorinated styrene butadiene rubber (Cl-SBR)/ zinc sulfide (ZnS) nanocomposites were prepared by a simple two-roll mill mixing technique. The interaction between the ZnS nanoparticles and Cl-SBR was assessed using Fourier transform infrared (FTIR) and UV-Vis spectroscopy, transmission electron microscopy (TEM), scanning electron microscopy (SEM), energy dispersive X-ray (EDX), X-ray diffraction (XRD), and thermogravimetric analysis (TGA). The dielectric constant, oil resistance, flame retardancy and the transport properties of nanocomposites with aromatic hydrocarbons were also analyzed with special attention to the loading of nanoparticles. The spectroscopic studies revealed the existence of a strong interfacial interaction between rubber chain and ZnS nanoparticles. TEM analysis showed the attachment of ZnS nanoparticles in the chlorinated SBR having nanosize region. SEM and XRD showed the uniform arrangement of nanoparticles in the elastomeric network. The presence of ZnS nanoparticles in the rubber matrix was confirmed through EDX spectroscopy. The thermal stability, flame retardancy and oil resistance properties of the nanocomposites were significantly enhanced by the addition of nanoparticles. Composite with 7 phr loading showed the maximum dielectric constant and beyond this loading, the dielectric property decreased due to the agglomeration of nanoparticles. Transport behavior of nanocomposites in benzene, toluene and xylene were analyzed in the temperature range of 27 to 70 °C. Swelling parameters such as rate constant, sorption, diffusion, and permeation coefficient were estimated. The mechanism of transport of the aromatic solvents in the filled Cl-SBR was found to be following anomalous mode. Temperature dependence of diffusion was used to study the activation parameters of the prepared samples.

Keywords Cl-SBR · Zinc sulfide nanoparticles · Crystallinity · Flame retardancy · Oil resistance · Thermal stability · Dielectric property · Transport properties · Aromatic solvents

Introduction

Elastomeric materials and composites have served modern society for decades. These materials are used in various industrial applications including transportation, construction, electrical cables, oil seals and packaging materials [1, 2]. However, the poor dispersion of filler particles in the polymer-

ic composites may corrode when exposed to moisture, hazardous solvents, UV radiation etc. This leads to the loss of mechanical properties and reduction in the lifetime of composite materials [3, 4]. The deterioration of the mechanical properties of the conventional polymeric composites can be overcome by incorporating nano-sized particles within the polymer matrix. The deterioration of mechanical properties depends on the size, the aspect ratio, degree of dispersion, and orientation of the nanoparticles in the rubber and the degree of adhesion of nanoparticles to the polymer chains [5–7]. One of the unique properties of nanocomposites, especially metal nanoparticles filled polymers is the low penetration of solvents and gases into the matrix. The solvent resistant polymeric films have strong potential applications in various fields. The properties of the solvent resistant membrane depend on the transport in polymers, their molecular properties,

✉ M. T. Ramesan
mtramesan@hotmail.com

[1] Department of Chemistry, University of Calicut, Calicut University P.O., Malappuram, Kerala 673 635, India

[2] Chemical Engineering Department, NIT Calicut, Kozhikode, Kerala, India

nature of penetrates, solubility, and polymer morphology of the interface. Various research works were carried out to verify the importance of nanoparticles in diffusion studies. It is generally found that the incorporation of filler with polymer matrix reduces the diffusion and permeation process of hydrocarbons into polymer matrices [8–11].

Hybrid composites as a way to enhance the properties of composites have received considerable attention from researchers. The addition of inorganic nanoparticles to rubbers allow the modification of rubber in physical properties as well as the implementation of new features in the polymer matrix. The dielectric properties of the polymer can be improved by proper mixing of semiconducting materials with rubbers which is important for the fabrication of flexible electronic material in various applications such as microwave absorbers, automobile, and in chemical industries [12]. Metal nanoparticles play an important role in the damping of mechanical vibrations in machine bearings and in vehicle base frames. The use of metal nanoparticles reduces the vulcanization time of the rubber nanocomposites which is due to the easy thermal conductivity of the polymer matrix [13, 14]. Among the semiconducting metal sulfide nanoparticles, ZnS shows remarkable properties which can be used for various applications such as electroluminescence, field emitters, electro catalyst and biosensors [15].

SBR is the widely used rubber in the production of tires, footwear, belts, conveyor, hoses, adhesives, and flooring [16, 17]. Usually, the reinforcement of SBR with polar fillers leads to poor mechanical properties due to the poor interaction (polar- nonpolar interaction) between rubber and filler particles. Moreover, SBR vulcanizates have very poor resistance to oil, ozone, and tensile strength, which restrict their use in such fields. Modified forms of SBR and polar rubbers play a vital role in enhancing interaction between the filler particles and the elastomeric matrix. Chemically modified SBR with randomly distributed dichlorocarbene groups in the backbone of polymer reduces the degree of unsaturation in SBR [18, 19]. The introduction of chloro groups into the rubber showed an elevation of the glass transition temperature. The dichlorocarbene reaction using the alkaline hydrolysis of chloroform is stereospecific and hence the resultant chlorinated SBR (Cl-SBR) shows superior tensile strength compared to the pure SBR. Moreover, the oil resistance and flame retardancy of styrene butadiene rubber have been drastically enhanced by the dichlorocarbene reaction [20].

The present study was motivated by a desire to know how metal sulfide nanoparticles affect the thermal stability, flame retardancy, conductivity and transport properties of sulfur vulcanized chlorinated SBR. To the best of our knowledge, no report on the preparation and properties of Cl-SBR/ZnS nanocomposite is available. The present study focused on the development of a new class of sulfur vulcanized Cl-SBR/ZnS nanocomposites through a simple, inexpensive two roll mill

mixing technique. The nature of nanoparticles in the Cl-SBR matrix was determined by X-ray diffraction (XRD), transmission electron microscopy (TEM), scanning electron microscopy (SEM), and infrared spectroscopy. Here the effect of the nature of penetrant molecules, loading of nanoparticles, and the temperature on transport of solvent through Cl-SBR/ZnS matrix were evaluated. Also, the electrical properties, at various frequencies, will be discussed thoroughly. The thermal stability, dielectric properties, oil and flame resistance of the nanocomposites have been studied with respect to the different loading of nanoparticles.

Experimental

Materials and methods

Zinc sulphate, sodium sulfide and cetyl trimethyl ammonium bromide (CTAB), benzene, toluene and xylene were purchased from Merck India. SBR (Synaprene 1502) was purchased from Synthetics and Chemicals Ltd., India. Rubber ingredients such as zinc oxide (ZnO), stearic acid, 2, 2, 4-trimethyl-1,2-dihydroquinoline (TDQ), N-cyclohexyl-2-benzothiazole sulfenamide (CBS), tetramethyl thiuram disulfide (TMTD), processing oil and sulfur were used for fabrication of sulfur vulcanized Cl-SBR/ ZnS composites.

Preparation of zinc sulfide nanoparticles

ZnS nanoparticles were prepared using a hydrothermal method [21]. An equimolar ratio of $ZnSO_4.5H_2O$ and $Na_2S.7H_2O$ powder was dissolved separately in de-ionized water. The sodium sulfide solution was then added drop by drop to the $ZnSO_4$ solution with constant stirring. The white precipitate formed was charged into the Teflon-lined stainless steel autoclave and maintained at a temperature of 220 °C for 12 h., then cooled down to room temperature. De-ionized water, then alcohol was used to remove the impurities in the precipitate. The washing procedure was also repeated several times to remove impurities from samples. After washing the precipitate, it was dried at 60 °C in a vacuum oven for 12 h.

Preparation of chlorinated SBR

Chlorinated SBR with 15% chlorine content was prepared from SBR by the in situ reaction of chloroform with aqueous caustic soda using phase transfer catalysis (CTAB), as reported earlier [22]. Briefly, SBR was dissolved in toluene. The phase transfer catalyst (CTAB) was added to this and the solution was stirred well. $CHCl_3$ was added drop by drop followed by an aqueous NaOH solution. The chlorinated SBR was separated from the solution by coagulating it with isopropyl alcohol and dried.

Preparation of Cl-SBR/ZnS nanocomposites

Chlorinated SBR/ ZnS nanocomposites were prepared at room temperature using a two mill mixing technique. Compounding of Cl-SBR with different loadings of ZnS nanoparticles (0, 3, 5, 7, 10, and 15 parts per hundred parts rubber (phr)) were carried out in an open two roll mixing mill. The rotors operated at a speed ratio of 1:1.4. Rubber composites were prepared by adding 5.0 phr ZnO, 2.0 phr stearic acid, 1.0 phr TDQ, processing oil (1/20th of nanoparticles), 1.2 phr CBS, 0.8 phr TMTD, 2.2 phr sulfur to rubber. The vulcanization ingredients were added to the rubber before the addition of the nanoparticles. Finally, the sulfur was added. The compounding was carried out in accordance with the ASTM method with paying special attention to maintaining the uniform distribution of nanoparticles. The sample codes used for this study are CSZ_0 for Cl-SBR without ZnS, CSZ_3, CSZ_5, CSZ_7, CSZ_{10}, and CSZ_{15} are polymer composites with 3, 5, 7, 10 and 15phr of ZnS nanoparticles, respectively.

Characterizations

JASCO (Model 4100) Fourier Transform Infrared spectrophotometer was used to collect the Fourier Transform Infrared (FT-IR) spectra of the Cl-SBR and Cl-SBR/ZnS nanocomposites in the region of 4000–400 cm^{-1} by casting the unvulcanized sheet of rubber samples from toluene solutions between KBR windows of size 25×4 mm with 72 scans of 4 cm^{-1} resolution. The ultraviolet-visible (UV-vis) absorption spectra of unvulcanized Cl-SBR/ZnS nanocomposites in toluene were recorded by a Perkin Elmer Lambda 650 spectrophotometer. The X-ray diffraction patterns of the composite materials were collected using Bruker AXS D X-ray diffractometer using CuKα radiation (k = 1.5406 Å) with an accelerating voltage of 30 KV. The diffractograms were recorded in the range of $2\theta = 10$ to 80° with 2 °/min step. The structure of composite was analyzed by a transmission electron microscopy (TEM). Ultra-thin sections of the specimen for the TEM were prepared by cutting the rubber samples with a Reichert Ultracut E ultramicrotome at about −100 °C and the images were collected from a TEM Libra 200 model. The surface morphology and percentage elements composition of the samples were carried out by Field Emission Scanning Electron Microscope (FESEM) with Energy Dispersive X-ray Spectroscopy (EDX) (FEI- NOVA NANOSEM-430). The sample preparation was done putting the nanocomposite films on a carbon supported grid using a conductive carbon tape and a thin gold layer was coated on it by using sputter coating instrument (EMITACH). The thermal decomposition behavior of the nanocomposite was analyzed by Perkin Elmer thermogravimetric analyzer at a heating rate of 10 °C min^{-1} in a nitrogen atmosphere. The dielectric constant of the elastomeric materials was analyzed by automatic Hewlett Packard LCR

meter (HP: 4284A) in the frequency range 10^2 to 10^6 Hz. The flame retardancy of the composites was carried out by the limiting oxygen index (LOI) test using a Stanton Redcroft FTA flammability tester, under nitrogen–oxygen atmosphere as per ASTMD-2863. The thin sheets of the vulcanized samples with an overall length of 80 mm and width of 30 mm were used for the LOI analysis. The minimum concentration of the oxygen in the oxygen–nitrogen mixed gas environment just sufficient to sustain the flame for 30s is taken as the LOI:

$$LOI = \left[\frac{\text{volume of oxygen}}{\text{volume of oxygen + volume of nitrogen}} \right] \times 100 \qquad (1)$$

The sulfur vulcanized samples of ZnS/chlorinated SBR composites were immersed in ASTM # 1, 2 and 3 oils at different temperatures. After 72 h of oil immersion, the samples were removed, then dipped in acetone and wiped off with filter paper to remove excess oil from the surface. From the relative weight difference of the samples, the oil resistance of Cl-SBR composite was assessed. The solvent penetration and transport behavior of Cl-SBR/ZnS nanocomposites were carried out by cutting circular-shaped samples from the vulcanized sheet. The sample thickness was measured accurately. Before the test, samples were weighed and then immersed in various solvents like benzene, toluene, and xylene in the diffusion flask. The weight of the samples was taken at different time intervals and again immersed in the corresponding solvents. The weighing process of rubber vulcanizate was continued until an equilibrium stage was obtained. The solvent uptake measurements were repeated with the same solvents at various temperatures.

Results and discussion

FTIR spectra

Fourier transform infrared spectroscopy (FTIR) has been employed for examining the interaction of nanoparticles with the functional groups in the elastomer. Figure 1 presents the FTIR spectra of ZnS, chlorinated SBR, and SBR/ ZnS composite. The different spectral assignments obtained from the infrared bands of polymeric materials are summarized in Table 1. The IR spectra of ZnS showed a strong absorption peak at 615 cm^{-1}, corresponding to the ZnS particles. The spectra of ZnS also showed two additional peaks at 3487 cm^{-1} and 1619 cm^{-1}, corresponding to the stretching and bending vibration of -OH group on the surface of metal sulfide particles [23]. The spectrum of Cl-SBR showed the C-H stretching at 2930 and 2853 cm^{-1}. Also, the CH_2 in-plane deformation and the *trans* C=C stretching of SBR has observed at 1443 and 968 cm^{-1}, respectively. Moreover, the aromatic stretching vibration appears at 700 cm^{-1}. The absorption band at 804 cm^{-1} and 1067 cm^{-1} are the corresponding C-Cl stretching and the
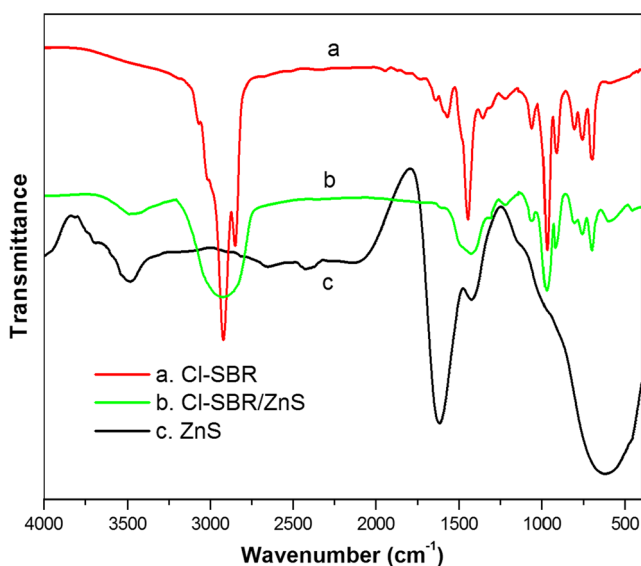
Fig. 1 FTIR spectra of ZnS, Cl-SBR and ZnS filled Cl-SBR

cyclopropyl ring of chlorinated SBR, respectively [22]. The Cl-SBR/ ZnS composite exhibited all the absorption peaks of elastomer with the typical stretching of ZnS particles. The composite showed the typical ZnS absorption at 588 cm^{-1} suggests the

Table 1   Assignments of the infrared bands of Cl-SBR, ZnS and Cl-SBR/ZnS nanocomposite

Materials	Wavenumber (cm^{-1})	Assignments
Cl-SBR	2930 and 2853	$\upsilon(CH_3-, -CH_2, >CH-)$ asymmetric stretching
	1566	$\delta(-CH_2-)$ bending vibration
	1443	$trans-CH=$
	1067	cyclopropyl ring
	968	$trans-CH=$
	912	vinyl 1,2 content
	804	C-Cl stretching
	752	C–H out of plane deformation of vinyl
	700	aromatic stretching vibration
ZnS	3487	OH stretching
	1619	OH bending
	615	Zn-S stretching
Cl-SBR/ZnS	3480	OH stretching
	2926	CH$_2$ stretching
	1419	$trans-CH=$
	1060	cyclopropyl ring
	970	$trans-CH=$
	918	vinyl 1,2 content
	808	C-Cl stretching
	700	aromatic stretching vibration
	588	Zn-S stretching

insertion of nanoparticles in the polymer. Moreover, the stretching vibration of C-H groups in SBR (at 2930 and 2853 cm^{-1}) are overlapped and merged to a broad absorption band at 2926 cm^{-1} as a result of ZnS particles insertion. In addition to this, the CH$_2$ absorption peaks (1443 cm^{-1}) of SBR is slightly shifted to lower frequencies (1419 cm^{-1}). The shift in peaks and the broadness of absorption bands in Cl-SBR/ ZnS composite is due to the strong interfacial interaction between the polymer and nanoparticles, suggesting that the absorption frequencies of nanocomposites are strongly influenced by the insertion of nanoparticles. This result is in good agreement with our previous studies [24, 25]. The mechanism of the interaction of nanoparticles with the chlorinated SBR is given in Scheme 1.

UV-Vis spectra

The UV-Vis spectrum of Cl-SBR and different contents of ZnS/ Cl-SBR nanocomposites are shown in Fig. 2. The UV spectra of Cl-SBR observed at 287 is due to the π to π* transition of the polymer [26]. However, the n-π* transition of Cl-SBR is found to shifting to a higher wavelength region for all the composites. Interestingly, the intensity and broadness of all the composites are significantly higher than that of pure Cl-SBR. This is another evidence for the insertion of nanoparticles into the elastomeric system. Additionally, the absorption edge of all nanocomposites is higher than Cl-SBR in the entire range of UV absorbance from 200 to 700 nm. Among the nanocomposite, the intensity and broad of UV peak is maximum at 7 phr loading. This means that the interfacial interaction between filler and polymer is maximum at this loading. The decrease in broadness and intensity of UV peak beyond 7 phr loading is due to the agglomeration of nanoparticles, which prevents the easy passage of light energy through the polymer matrix and these results are in accordance with the recent studies [24, 25].

X-ray diffraction analysis (XRD)

X-ray diffraction patterns of ZnS, Cl-SBR and Cl-SBR/ZnS nanocomposites are displayed in Fig. 3. The XRD pattern of ZnS exhibits the crystalline peaks at 29.6°, 48.23° and 56.97° corresponding to the diffraction of (111), (220), and (311) crystal planes of pure ZnS respectively [27]. All peaks are indicative of ZnS without any impurity indicating the high purity of the synthesized compound. The XRD of Cl-SBR vulcanizate showed strong diffraction peak at 2θ = 21.2° in addition to the crystalline peak at 2θ = 29.36°. The XRD of nano- ZnS embedded Cl-SBR vulcanizate exhibited the characteristic peaks of polymer with the crystalline peaks of ZnS. It is evident from the figure that the addition of nanoparticles to Cl-SBR affected the structure of the composite, which was clearly reflected through the shift in diffraction peak to a lower diffraction angle

Scheme 1 The mechanism of interaction between nanoparticles and Cl-SBR
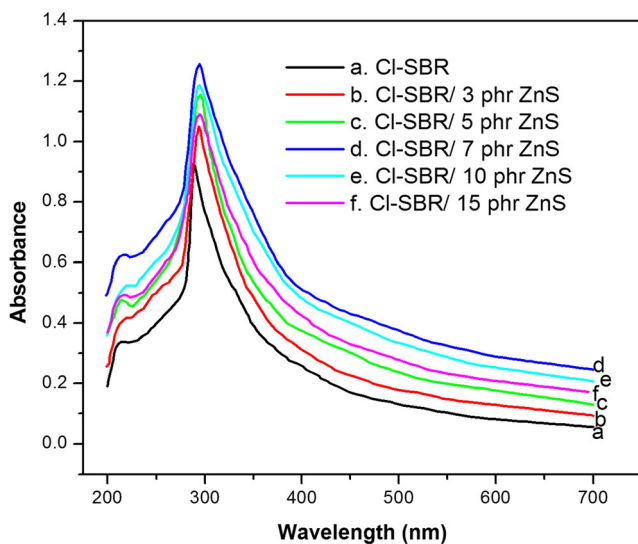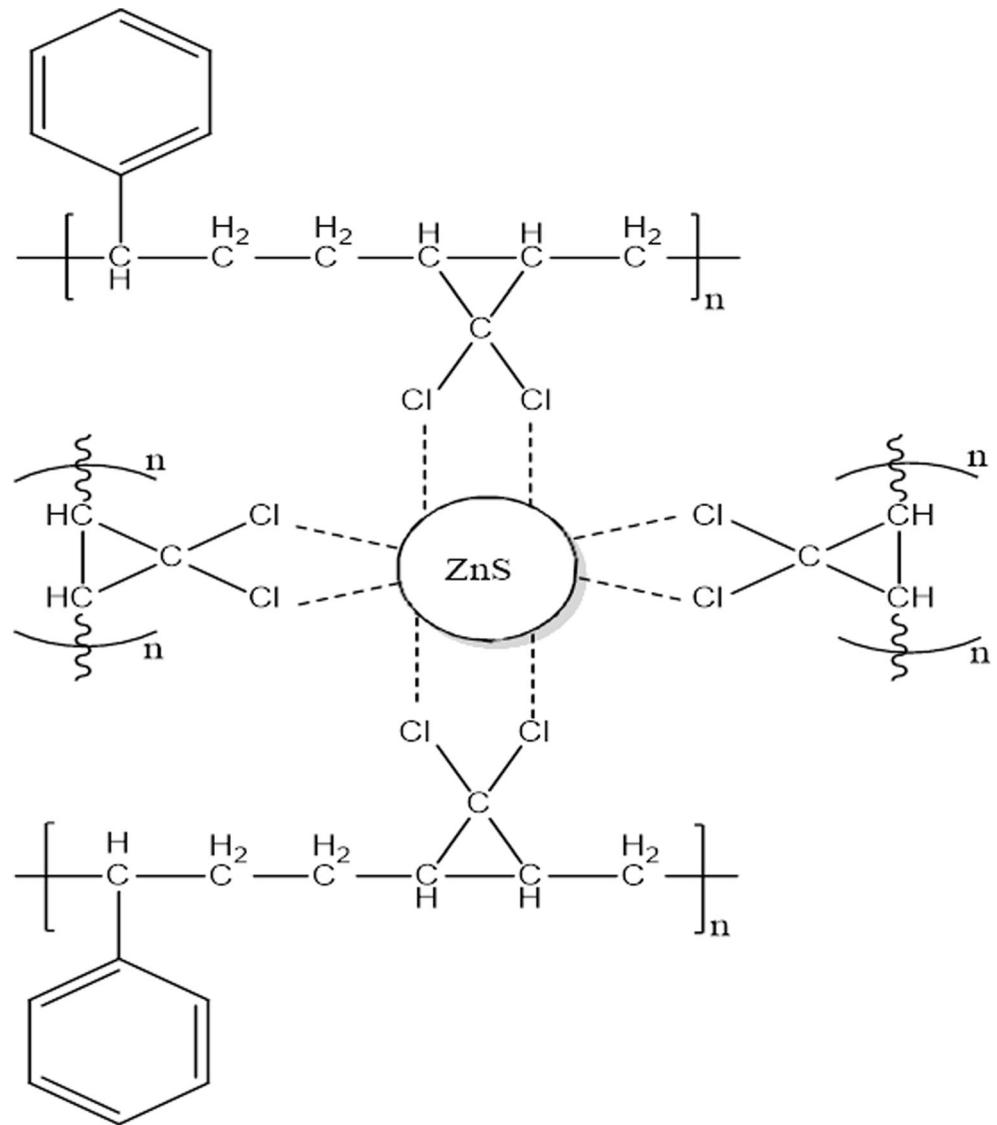
**Fig. 2** UV spectra of Cl-SBR with different contents of ZnS nanoparticles

compared to that of pure ZnS. It is evident from the figure that the broadness of the amorphous peak of Cl-SBR is greatly reduced by the addition of ZnS nanoparticles.

Transmission electron microscopy (TEM)

Figure 4 shows the TEM images of ZnS, rubber nanocomposite with 7 and 15 wt.% of ZnS particles. The TEM micrograph (Fig. 4a of the prepared ZnS powder shows several spherical shaped nano-crystals with an average size of 2 to 15 nm. The Fig. 4b shows the uniform distribution of metal sulfide particles with various sizes ranging from 30 to 60 nm within the chlorinated SBR matrix. The uniform nature of nanocomposite is due to the strong interfacial adhesion between the chlorinated SBR and ZnS nanoparticles. However, the morphology of the composite (Fig. 4c) is remarkably changed into an elongated structure with the aggregation of nanoparticles

Fig. 3 XRD pattern of ZnS, Cl-SBR with different contents of ZnS
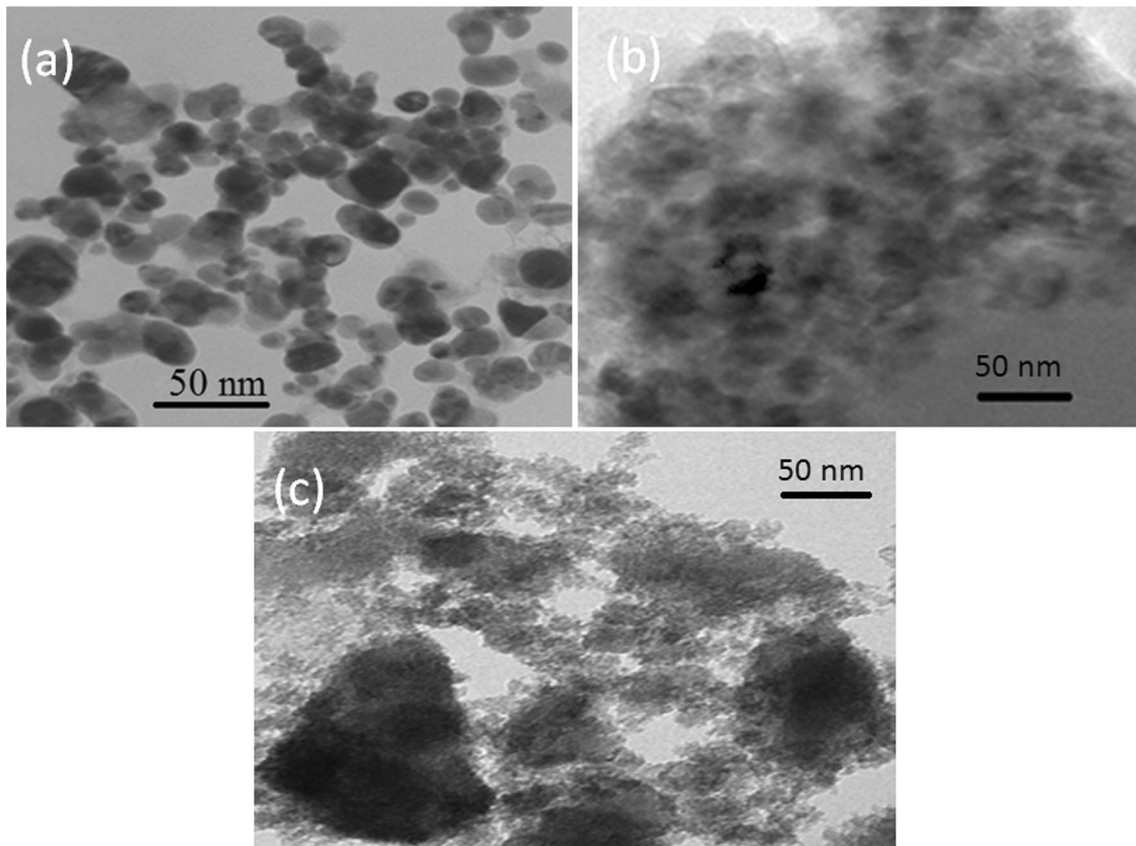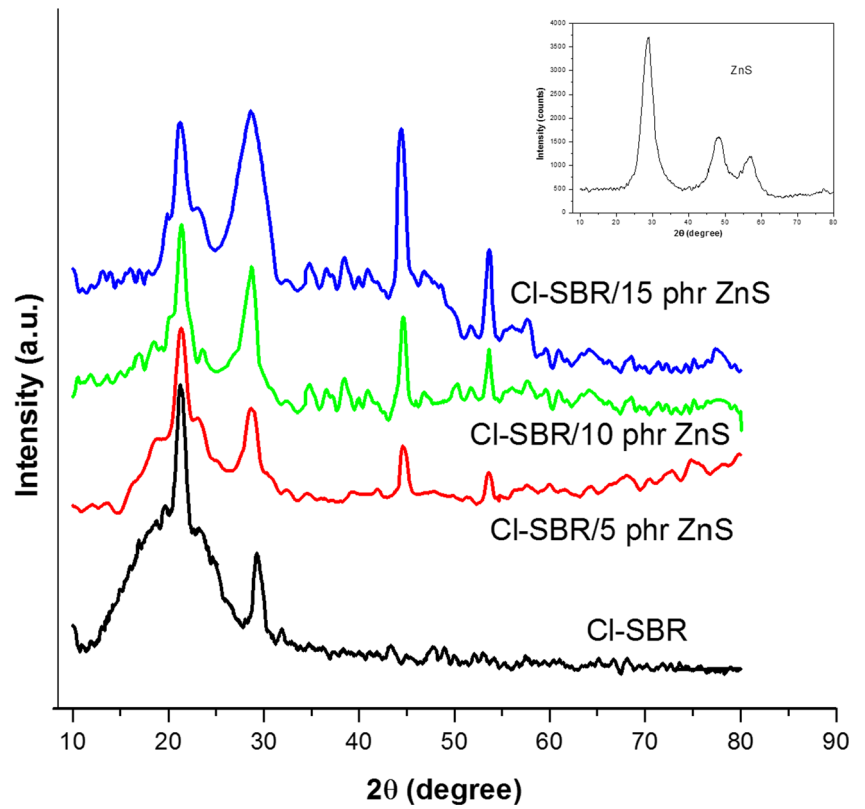
Fig. 4 TEM images of (**a**) ZnS (**b**) Cl-SBR/7 phr ZnS and (**c**) Cl-SBR/15 phr ZnS

indicating the poor interaction between of nanoparticles with the rubber matrix.

Scanning electron microscopy (SEM)

Figure 5 shows the SEM photographs of Cl-SBR and the different loading of ZnS-filled Cl-SBR. The SEM image of Cl-SBR has a rough morphology with frequent ridgelines indicating the direction of crack propagation. The irregular morphology of the chlorinated SBR is completely changed into a very smooth surface with embedded nanoparticles as shown in Fig. 5b. These particles are uniformly distributed in the Cl-SBR matrix with an average size ranging from 60 nm to 90 nm. The uniform dispersion of nanoparticles in the polymer matrix is due to the strong interfacial interaction between the filler and the polar segments of Cl-SBR. When the loading of nanoparticles reaches to 15 phr (Fig. 5c), the domain size of the dispersed phase remarkably increased due to the poor interaction of nanoparticles with Cl-SBR. This leads to the agglomeration of fillers within the macromolecular chain of Cl-SBR matrix. The percentage of chemical elements of Cl-SBR/15 wt.% ZnS nanocomposite in a particular area of SEM image (Fig. 6) is given in Table 2. Presence of C, Cl, Zn and S elements in EDX spectrum indicates that ZnS nanoparticles

are dispersed in the Cl-SBR matrix. The presence O may be due to the -OH moieties present in the surface of ZnS particles.

Thermogravimetric analysis (TGA)

The thermal behavior of Cl-SBR nanocomposites with various loadings of ZnS was investigated using TGA and the results are presented in Fig. 7. It can be seen that all the samples showed two plateaus, suggesting two stages of weight losses. The initial weight loss below 250 °C is due to the ingredients of the compound and the removal of HCl from the elastomeric chain. The second thermal degradation from 380 °C to 560 °C is a continuous weight loss, which can be attributed to the decomposition of the SBR chain [28]. It is also clear that the initial and final decomposition temperatures of Cl-SBR/ZnS nanocomposites are higher than that of the parent polymer, which reveals the high thermal stability of the fabricated composites. The thermal stability usually depends on the crystalline nature of the filler particles and the uniform dispersion of nanoparticles in the polymer matrix. The increased thermal stability with the filler loading is due to the interaction between the nanoparticles and polymer segments. Moreover, the metal sulfide nanoparticles retarded the motion of the elastomeric chains, acting as a protective layer
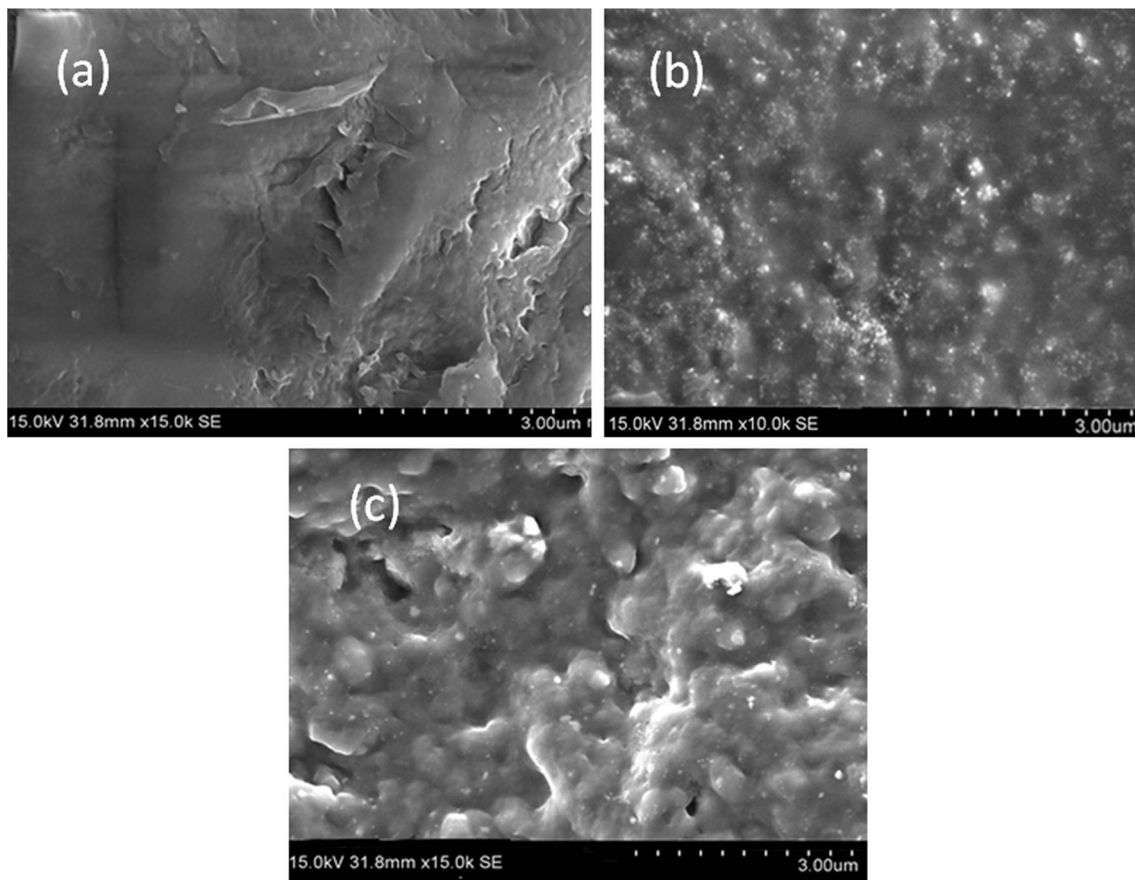
Fig. 5 SEM images of (**a**) Cl- SBR (**b**) Cl-SBR with 7 phr and (**c**) Cl-SBR with 15 phr ZnS

Full Area 2 - Det 1
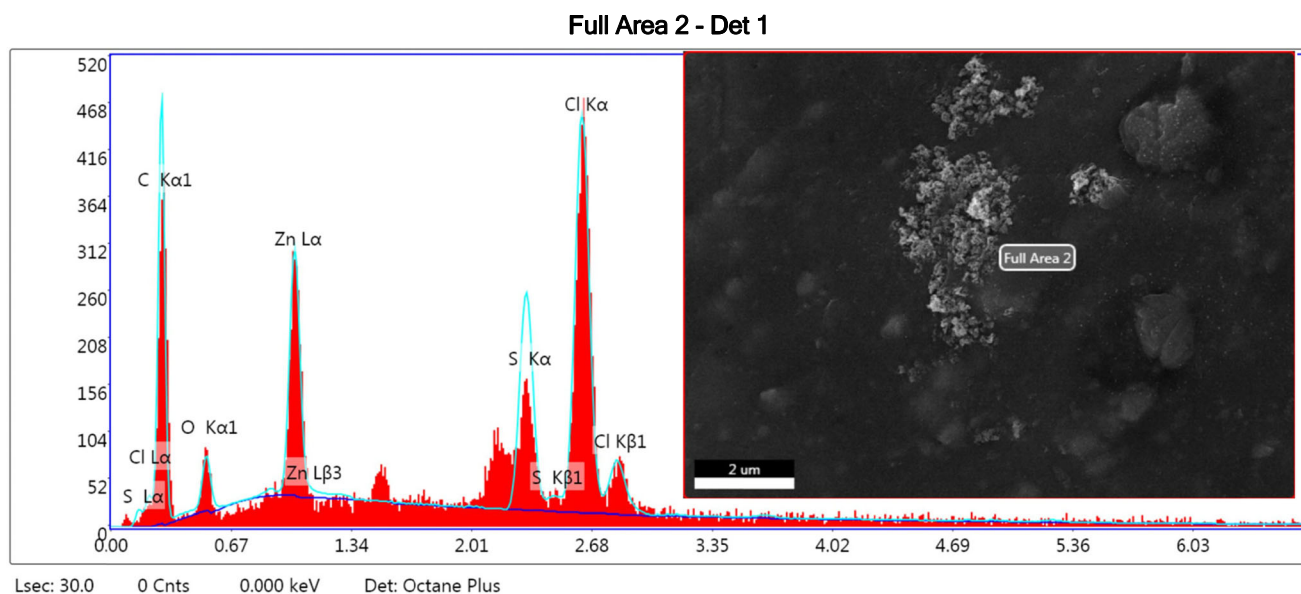
Fig. 6 EDX and the SEM image of Cl-SBR/15 phr ZnS composite

on the surface of the matrix, which prevents the thermal degrading of the polymer and enhanced the thermal stability of the nanocomposites. The final char residue obtained at 600 °C for Cl-SBR is only 6.87% whereas the composite with 5, 10 and 15 phr nanocomposite shows the final char residue around 11.26, 17.03 and 21.92%, respectively, at the same temperature. The char formed after the thermal decomposition of the polymer matrix is an important factor which significantly improves the flame retardant behavior of the nanocomposite [29]. Here, the increased char residue of the nanocomposite with the increase in concentration of nanoparticles indicates the enhanced flame resistance of the composite materials [24, 25]. This result will be further substantiated with the help of the LOI values of the composites.
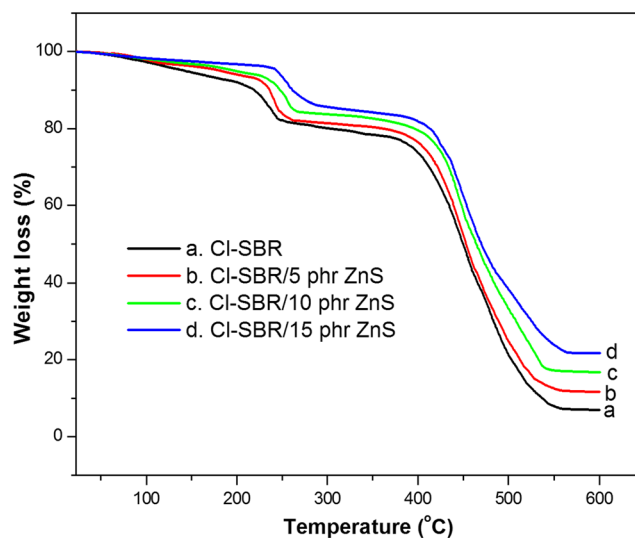
Flame retardancy

Limiting oxygen index (LOI) is one of the major qualitative methods to analyze the flame resistance behavior or fire performance of elastomeric materials. LOI is the minimum content of oxygen required in a nitrogen/ oxygen mixture of a self-sustained combustion of any material [30]. The LOI value of Cl –SBR and its nanocomposites with different loadings of ZnS nanoparticles are given in Fig. 8. The presence of dichloro groups in Cl-SBR

affected the flammability and this is due to the intumescences effect. The chlorine containing heavy gases produced during combustion of Cl-SBR reduced the access of oxygen and consequently suppresses the flame propagation of the polymer matrix. Halogen-containing species usually act in the vapour phase by capturing the radicals to interrupt the oxidative flame chemical processes and thus suppress the combustion of the polymer. It is well known that the fire resistance of polymeric composites depends on the nano-filler distribution and the synergistic interaction between the nano-filler and polymer. In the present study, the increased LOI value with the addition of nanoparticles is due to the strong interfacial interaction between the polar units of Cl-SBR with the ZnS nanoparticles. Also, the metal particles present in the nanoparticles reduces the carbonization of rubber

Table 2 Percentage of element composition in Cl-SBR/ZnS nanocomposite

Element	Weight %	Atomic %
C K	51.67	75.69
O K	3.52	3.87
Zn L	10.15	2.73
S K	9.71	5.33
Cl K	24.95	12.38

Fig. 7 TGA curve of Cl-SBR and Cl-SBR with different contents of ZnS nanoparticles
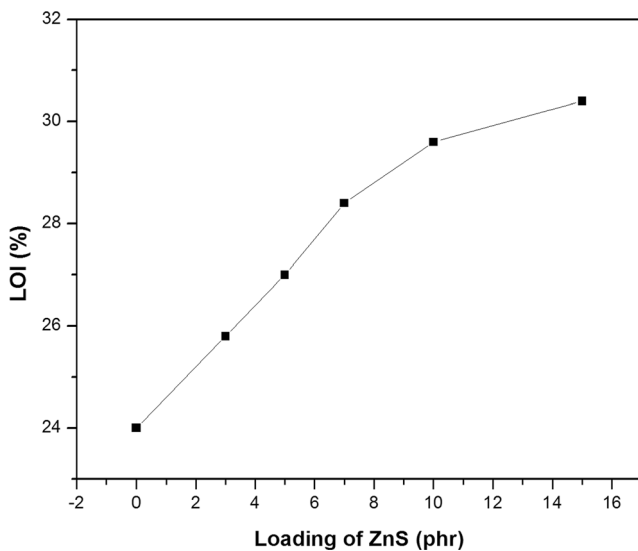
Fig. 8 Flame resistance of Cl-SBR and Cl-SBR/ZnS nanocomposites

generating more protective char layer, which resists the transfer of heat and fuel and thereby inhibiting flammability [31].

Dielectric constant

The dielectric properties of polymer composites are determined by its molecular structures. Dielectric constant recorded as a function of frequency, at room temperature, for Cl-SBR/ZnS nanocomposites is plotted in Fig. 9. It can be observed that the dielectric constant of all the composites is greater than the pure chlorinated SBR. This means that the nanocomposites are greatly polarized more than that of Cl-SBR. The enhancement in dielectric constant is ascribed to the interfacial polarization phenomenon developed in the heterogeneous materials that have different conductivity stages. The interfacial polarization of composite usually decreases with increasing
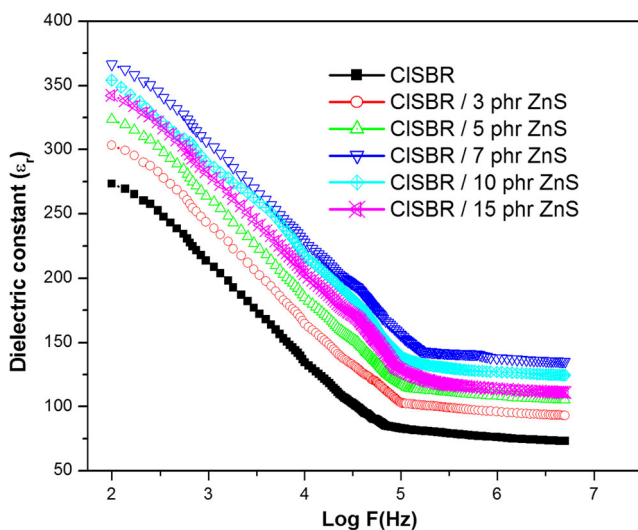

Fig. 9 Dielectric constant of Cl-SBR and different contents of nano-ZnS filled Cl-SBR

the frequencies. The charge carriers developed by the application of electric field are completely oriented in a uniform direction, which results in interfacial polarization and consequently the dielectric constant is high at lower frequencies. However at higher frequencies, the electron exchange among the charge carriers cannot be oriented in the direction of the applied field and, therefore, the resultant dielectric constant is always lower, indicating the poor interfacial polarization in polymer composites [32]. The dielectric constant of polymer composites is directly related to the molecular structures, polarizations, and interfacial interactions between the filler particles and polymeric chain. The dielectric constant of 7 phr Cl-SBR/ZnS composite is significantly higher than that of other four composites in the entire range of frequencies. The high dielectric value is due to the formation of uniform clusters. A cluster may be considered as a region where the nanoparticles and the elastomer stick together uniformly or are very close to each other because of the interfacial interaction or polar-polar interaction between the filler and the polymer matrix. In the present study, the average polarization associated with the uniform cluster is maximum in 7 phr loading. The increased interfacial interaction facilitates the orientation of dipoles, thereby leading to an increase in the dielectric values. The decrease in the dielectric constant of the composite beyond 7 phr loading can be explained by the poor interaction of filler and polymer and also with the agglomeration of nanoparticles. It is well known that the segmental mobility of the polymer decreases with the loading of nanoparticles and therefore the dielectric property decreases at higher loading.

Oil resistance

Transport of oil and fuel through elastomers is the major controlling factor in many of the barrier applications in the automobile industry, since a variety of spare parts may be exposed to oils, fuels and greases [31]. Figure 10 shows the resistance of the chlorinated SBR and its nanocomposites to ASTM oil. It can be observed that the percentage of oil uptake is significantly decreased after the addition of ZnS nanoparticles to chlorinated SBR. The oil resistance of rubber depends on the electronegativity of rubbers, crystallinity, crosslink density in the matrix, and polarity of the solvent. The oil resistance of the composites decreases with the loading of nanoparticles up to 7 phr loading. This can be attributed to the fact that the effective interaction of crystalline ZnS with chlorinated rubber restricts the penetration of oil into the intermolecular spaces and hence decreases the swelling percentage [32]. On increasing the loading of nanoparticles (above 7 phr), the oil resistance is found to be decreasing and this is due to the loosely bound filler particles in the polymer matrix. The oil resistance of all the vulcanizates is found to be increasing with the increases in temperatures, as more solvent could penetrate inside the polymeric matrix.
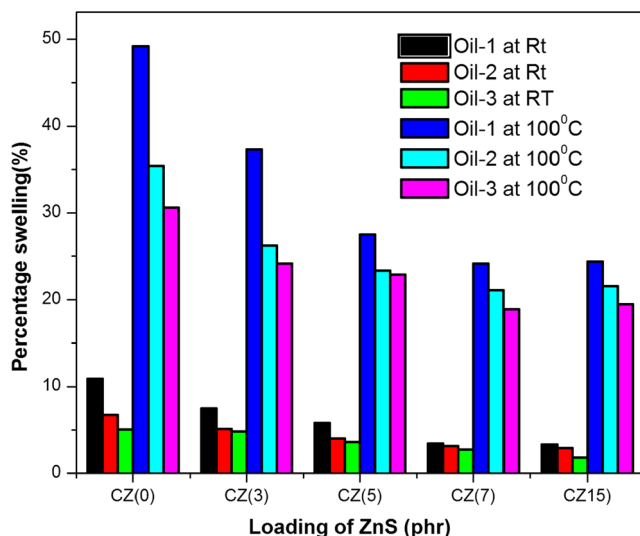
Fig. 10 Oil resistance properties of Cl-SBR and Cl-SBR/ZnS nanocomposites at different temperatures

Fig. 11 Sorption curves of different loading of ZnS in Cl-SBR with benzene

Diffusion experiments

The diffusion studies were done using the sulfur vulcanized samples; both weight and thickness of these samples were measured accurately. Initially, samples were soaked in about 20–25 ml of solvents in diffusion bottles, and were closed and put in the thermostatically controlled oven for particular time intervals. The samples were weighed out at regular intervals and put back in the bottles. Samples were weighed until equilibrium weight was obtained [33].
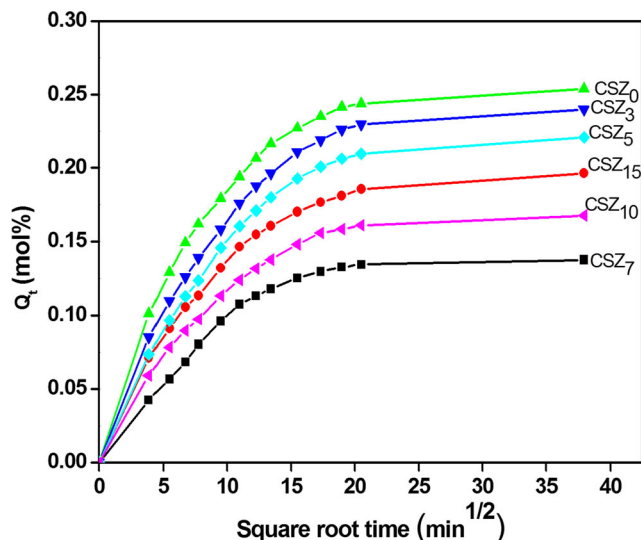
The diffusion of different solvents through various nanocomposites was studied. The percentage uptake of solvents was calculated using:

$$Q_t \,(mol\%) = \frac{\text{Mass of solvent sorbed/Molar mass of solvent}}{\text{Mass of polymer}} \times 100 \quad (2)$$

The percentage uptake (Q_t %) of different solvents were plotted against the square root of the time. The mol uptake of solvents depends on the filler content, temperature and molecular weight of solvents.

Effect of ZnS concentration on mol uptake

The influence of ZnS nanoparticles on the mol uptake of benzene through Cl-SBR/ZnS nanocomposites at room temperature is presented in Fig. 11. All the solvents show the same trend and the decrease in diffusion and sorption of the nanocomposites is due to the increased interfacial interaction between the nanoparticles and the macromolecular chain of the polymer. Upon addition of fillers, the local mobility of polymer segments are restricted, thus the flexibility of polymer gets lowered, which leads to the decreased sorption [34]. The better distribution of ZnS nanoparticles in the Cl-SBR matrix enhances the surface area of the reinforcing phase. At lower concentrations of

loading, the penetrant molecules can pass through the matrix very easily due to the homogeneous distribution of filler particles. The composite with 7 phr of ZnS showed minimum swelling and the unfilled matrix showed the highest sorption. The solvent uptake of polymer matrix varies with reference to the free volume inside the matrix. By the addition of filler, free volume inside the matrix lowers, which in turn decreases the equilibrium uptake of solvent.

The nature of solvent on sorption behavior

The effect of penetrant size was studied using aromatic solvents like benzene, toluene and xylene and the results are summarized in Fig. 12. It is seen that benzene shows the maximum and xylene shows the minimum sorption and the toluene lies in between. As penetrant size increases, the diffusivity values
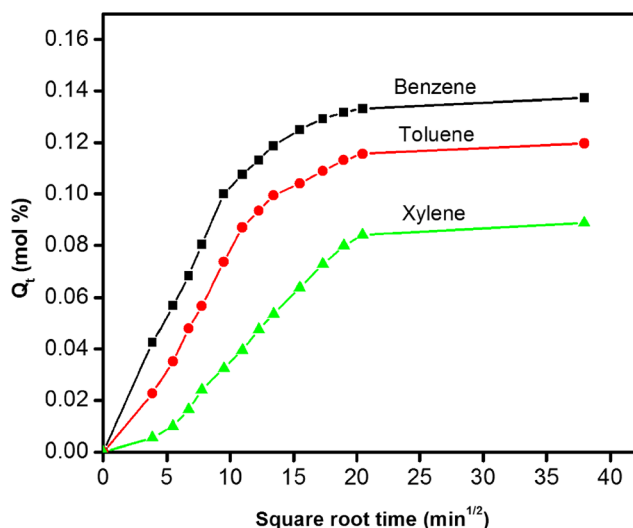
Fig. 12 Solvent uptake of Cl-SBR with 7phr of ZnS in different aromatic solvents

decreases, which can be explained on the basis of free volume theory [35]. According to the free volume theory, the rate of diffusion depends on the ease of exchange of polymer segments and their positions with the penetrant molecules. As the molar volume of solvent increases, the exchange of polymer segments becomes difficult. It is well recognized that the solvent uptake decreases with increase in reinforcement of filler particles in the polymer matrix. The activation energy needed for the sorption of large molecules is very high, which is the reason for a decrease in the solvent uptake.

Mechanism of sorption

The transport mechanism can be calculated using the equation [36].

$$\log \frac{Q_t}{Q_\infty} = \log k + n \log t \tag{3}$$

where Q_t is the mole percent uptake of solvent, k is a constant, which depends on the structural parameters and the interaction between solvent and matrix, n represents the mode of transport. On regression analysis, the value of n and k are obtained. The transport is called Fickian, when the value of $n = 0.5$, where the chain relaxation of the polymer chain is higher than that of the rate of diffusion of the solvent. If $n = 1$, the mode of transport is called non-Fickian, in which the penetration of the solvent is higher than that of polymer chain relaxation [37]. In this study, the value of n is in between 0.5 and 1, hence the mode of transport is called anomalous. The anomalous mode of transport can be due to: (1) the occurrence of a slow and viscous polymer chain relaxation upon reinforcement with the filler and (2) the coupling between Fickian and non-Fickian. From the Table 3, it is found that the value of n is approaching 1, which means the transport mechanism changed anomalous mode to non-Fickian mode [38]. The structural property of the polymer is obtained from the value of k. It also provides an idea about the interaction between a polymer matrix and penetrant molecules. Nanocomposites have a lower value of k as compared to the pure matrix, indicating the interaction between the solvent and the penetrant. A composite with 7 phr ZnS showed the lowest k value, which is due to the uniform distribution of nanoparticles in the polymer matrix.

Diffusion (D), sorption (S) and permeation (P) coefficients

Table 4 summarizes the coefficient of diffusion, sorption, and permeation of Cl-SBR ZnS nanocomposites in aromatic solvents. The coefficient of diffusion is a kinetic parameter related to the segmental motion of the polymer matrix, from which the rate of diffusion can be evaluated. According to Fickian law, the coefficient of diffusion can be calculated as the ratio of the diffusing substance per unit area of cross-section to the space gradient of the concentration using [39]

$$D = \pi \left[\frac{h\theta}{4Q_\infty} \right]^2 \tag{4}$$

where h is the thickness of the polymer sample, θ is the slope of the linear portion of the graphs of Qt against square root time. The diffusion coefficient decreases with the loading of nanoparticles and the lowest value have obtained for composite with 7 phr of ZnS nanoparticles. The reduction of free volume by the addition of the filler is due to the decrease in free volume within the matrix and a better distribution of nanoparticles in the polymer matrix. It is also seen that the diffusion coefficient values decrease when going from benzene to xylene. Generally, high activation energy is needed for large molecules to create free volume in the polymer matrix [40].

Diffusivity and sorption govern the permeation of solvent molecules into the polymer chain. The sorption coefficient can be calculated as the ratio of mass of solvent at equilibrium (M_s) to the mass of polymer sample (M_p), i.e., $S = M_s/M_p$. Permeation coefficient (P) is obtained by multiplying sorption and diffusion coefficients, i.e., $P = DS$. Permeation coefficient provides an idea about the solvent permeated into the uniform area of a polymer sample in one second. The coefficient of

Table 3 n and k values of Cl-SBR/ZnS with different filler loadings in aromatic solvents at room temperature

Samples	Benzene		Toluene		Xylene	
	n	$K \times 10^2 (\text{min}^{-1})$	n	$k \times 10^2 (\text{min}^{-1})$	n	$K \times 10^2 (\text{min}^{-1})$
CSZ0	0.54	0.16	0.63	0.12	0.72	0.11
CSZ3	0.57	0.14	0.69	0.11	0.79	0.09
CSZ5	0.62	0.12	0.76	0.09	0.83	0.07
CSZ7	0.79	0.04	0.89	0.05	0.96	0.03
CSZ10	0.73	0.09	0.84	0.07	0.89	0.05
CSZ15	0.71	0.11	0.81	0.08	0.87	0.06

**Table 4**   D, S and P values of Cl-SBR/ ZnS nanocomposites in aromatic solvents

Samples	Diffusion coefficient $D \times 10^5$ (cm²/s)			Sorption coefficient S (mol %)			Permeation coefficient $P \times 10^5$ (cm²/s)		
	Benzene	Toluene	Xylene	Benzene	Toluene	Xylene	Benzene	Toluene	Xylene
CSZ_0	1.72	1.61	1.38	1.18	1.13	1.09	2.03	1.81	1.50
CSZ_3	1.57	1.51	1.32	1.15	1.09	1.06	1.81	1.64	1.39
CSZ_5	1.48	1.39	1.27	1.11	1.06	1.02	1.64	1.47	1.29
CSZ_7	1.15	1.13	1.07	1.04	1.01	0.92	1.19	1.14	0.98
CSZ_{10}	1.37	1.24	1.19	1.09	1.04	0.97	1.49	1.28	1.15
CSZ_{15}	1.39	1.29	1.21	1.11	1.05	0.99	1.54	1.35	1.19

sorption, diffusion, and permeation of all the solvents through nanocomposite with different contents of ZnS show a similar trend as summarized in Table 4.

Effect of temperature on sorption behavior

The effect of temperature on diffusion studies is done at three different temperatures, 27, 50 and 70 °C. Composite with 7 phr of ZnS is shown in Fig. 13. The sample CSZ_7 (Cl-SBR/ 7phr ZnS) has selected to study the effect of temperature on benzene because it possesses the highest solvent resistance at room temperature. The mol uptake increases as the temperature increases. This is due to: (1) the increase in free volume inside the matrix and (2) the increase in the kinetic energy and segmental motion of the polymer chain [41]. Using the values of D and P in these three temperatures, the activation energy of diffusion and permeation was calculated and summarized in Table 5. According to Arrhenius equation

$$X = X_0 \exp\left(\frac{-E_X}{RT}\right) \qquad (5)$$
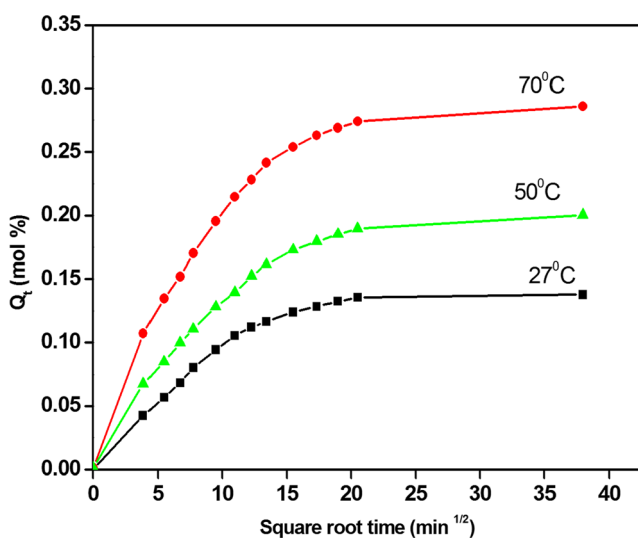
Fig. 13 The mole uptake of 7 phr ZnS/ Cl-SBR at different temperatures in benzene

where X is D or P, and X_0 is D_0 or P_0 and E_x is the activation energy of diffusion (E_D) and permeation (E_P). E_D and E_P correspond to the slope of the straight lines obtained by plotting log P and log D versus 1/T, respectively.

As the filler concentration and penetrant size increase, the activation energy also increases. For larger molecules, more space is needed to penetrate into the polymer matrix. The higher amount of energy is required to create free voids within the matrix and therefore the activation energy of diffusion and permeation increases. In the present study, CSZ_0 (pure matrix) showed the lowest and CSZ_7 (Cl-SBR with 7 phr of ZnS) showed the highest value of E_P and E_D values. The activation energies of diffusion and permeation are low at higher loading of nanoparticles, and this mainly due to the agglomeration of nanoparticles in the polymer.

Thermodynamic parameters

The thermodynamic properties such as enthalpy (ΔH_s) and entropy (ΔS_s) of sorption can be calculated from the Van't Hoff's relation [40]

$$\log K_s = \frac{\Delta S_s}{2.303R} - \frac{\Delta H_s}{2.303RT} \qquad (6)$$

where K_s is equilibrium sorption constant, which is the ratio of the number of moles of sorbed solvent at equilibrium to the mass

Table 5 E_D, and E_P values of CSBR/ZnS nanocomposites in aromatic solvents

Samples	Benzene		Toluene		Xylene	
	E_D	E_P	E_D	E_P	E_D	E_P
CSZ_0	6.24	5.26	6.42	5.28	6.67	5.46
CSZ_3	6.34	5.29	6.53	5.34	6.79	5.54
CSZ_5	6.48	5.32	6.64	5.47	6.89	5.63
CSZ_7	6.64	5.57	6.79	5.64	6.99	5.72
CSZ_{10}	6.59	5.54	6.76	5.59	6.96	5.68
CSZ_{15}	6.53	5.49	6.69	5.56	6.91	5.65

Table 6 ΔH, ΔS and ΔG of Cl-SBR/ZnS nanocomposites in aromatic solvents

Samples	ΔH(J/mol)			ΔS(J/mol/K)			$-\Delta G$(J/mol)		
	Benzene	Toluene	Xylene	Benzene	Toluene	Xylene	Benzene	Toluene	Xylene
CSZ_0	0.874	0.887	0.899	0.067	0.055	0.046	19.23	15.61	12.90
CSZ_3	0.879	0.892	0.907	0.063	0.051	0.041	18.02	14.41	11.39
CSZ_5	0.885	0.897	0.914	0.061	0.047	0.036	17.41	13.20	9.89
CSZ_7	0.899	0.917	0.929	0.052	0.041	0.027	14.70	11.38	7.17
CSZ_{10}	0.894	0.909	0.922	0.057	0.044	0.033	16.20	12.29	8.97
CSZ_{15}	0.892	0.905	0.919	0.059	0.046	0.035	16.80	12.89	9.58

of the polymer sample. The values of ΔH_s and ΔS_s are obtained by regression analysis of log Ks against 1/T. The values of ΔH_s obtained from E_P and E_D ($\Delta H = E_P\text{-}E_D$) values are in accordance with these values and are shown in Table 6. It can be seen that all the samples show positive values of ΔH_s, which is a clear indication of endothermic sorption. The entropy changes in all the samples are also positive, and are found to be decreasing upon the increase of filler loading. At higher loading, an increase in filler polymer contact occurs and causes a decrease in solvent diffusion. The free energy of sorption (ΔG_s) can be calculated from ΔH_s and ΔS_s values. The sample without the filler showed the minimum free energy of diffusion and CSZ_7 shows the maximum ΔG_s. It reveals that the diffusion of the matrix without filler is more spontaneous on comparing with its composites, that is, on adding the filler the ΔG_s values become less negative. This is a clear indication of the increase in the tortuosity of sorption through the polymer [42].

Conclusions

Cl-SBR/ZnS nanocomposites were prepared by a two-roll mill mixing method with different loading of ZnS nanoparticles and characterized by FTIR, UV, XRD, TEM, SEM, EDX, TGA, and impedance analyzer. The interfacial interaction between nanoparticles and Cl-SBR was confirmed from FTIR and UV spectrum by the shift in the absorption peaks of the polymer matrix. The XRD results indicated that the amorphous nature of Cl-SBR was decreased with the addition of nanoparticles. The TEM and SEM images revealed the presence of ZnS nanoparticles which were uniformly distributed in the elastomer at 7 phr loading. The attachment of ZnS nanoparticles in the chlorinated SBR was confirmed from EDX analysis. The thermal stability and flame retardancy were greatly enhanced with the addition of ZnS nanoparticles. Maximum dielectric constant was observed in samples with 7 phr of ZnS in Cl-SBR. Transport behavior of sulfur vulcanized composites in benzene, toluene and xylene were analyzed in the temperature range of 27 to 70 °C. Composite with 7 phr loading absorbed less solvent

and oils compared to those of other composites and with pure Cl-SBR, indicating a better interaction between filler and rubber. Transport properties such as diffusion coefficient, sorption coefficient and permeation coefficient have been estimated with respect to the loading of nanoparticles, nature of solvent and temperature. Diffusion coefficient decreases regularly in the order of xylene > toluene > benzene. The mechanism of diffusion was found to be Fickian in nature for Cl-SBR, while in the nanoparticles filled composites, it was anomalous.

References

1. Changjie Y, Zhang Q, Junwei G, Junping Z (2011) Cure characteristics and mechanical properties of styrene-butadiene rubber/hydrogenated acrylonitrile-butadiene rubber/silica composites. J Polym Res 18:2487–2494
2. Misha S, Shimpi NG, Patil UD (2007) Effect of nano CaCO3 on thermal properties of styrene butadiene rubber (SBR). J Polym Res 14:449–459
3. Wang J, Wu W, Wang W, Zhang J (2011) Preparation and characterization of hemp hurd powder filled SBR and EPDM elastomers. J Polym Res 18:1023–1032
4. Hong SG, Chan CK, Chuang CC, Keong CW, Hsueh YP (2005) The Curing behavior and adhesion strength of the epoxidized natural rubber modified epoxy/dicyandiamide system. J Polym Res 12:295–303
5. Jasna VC, Ramesan MT (2017) Studies on the mechanical, electrical properties and interaction of petroleum fuels with SBR/ manganous tungstate nanocomposites. J Inorg Organomet Polym Mater 27:968–978
6. Meng Y, Chu J, Liu C, Wei Z, Zhang L (2014) Oil resistance and mechanical properties of polysiloxane nanocomposites prepared by in situ reaction of reactive polar monomers. J Appl Polym Sci 131:1–11
7. Zhou X, Zhu Y, Gong Q, Liang J (2006) Preparation and properties of the powder SBR composites filled with CNTs by spray drying process. Mater Lett 60:3769–3775
8. Cosgrove T, Rodin V, Murray M, Buscall R (2007) Self-diffusion in solutions of carboxylated acrylic polymers as studied by pulsed field gradient NMR 1. solvent diffusion studies. J Polym Res 12:295–303
9. Abraham J, Maria HJ, George SC, Kalarikkal N, Thomas S (2015) Transport characteristics of organic solvents through carbon

nanotube filled styrene butadiene rubber nanocomposites: the influence of rubber–filler interaction, the degree of reinforcement and morphology. Phys Chem Chem Phys 17:11217–11228

10. Unnikrishnan G, Thomas S, Varghese S (1996) Sorption and diffusion of aromatic hydrocarbons through filled natural rubber. Polymer 37:2687–2693

11. Johnson T, Thomas S (1999) Natural rubber/epoxidised natural rubber-25 blends: morphology, transport phenomena and mechanical properties. J Mater Sci 34:3221–3239

12. Olivati CA, Carvalho AJF, Balogh DT, Faria RM (2006) Electrical properties of polymer/metal interface in polymer light-emitting devices: electron injection barrier suppression. J Mater Sci 41:2767–2770

13. Alwaan IM, Hassan A (2014) Effects of zinc borate loading on thermal stability, flammability, crystallization properties of magnesium oxide/(90/10) mLLDPE/(NR/ENR-50) blends. Iran Polym J 2:277–287

14. Mamunya YP, Davydenko VV, Pissis P, Lebedev EV (2002) Electrical and thermal conductivity of polymers filled with metal powders. Eur Polym J 38:1887–1897

15. Ogata T, Hirakawa N, Nakashima Y, Kuwahara Y, Kurihara S (2014) Fabrication of polymer/ZnS nanoparticle composites by matrix-mediated synthesis. React Funct Polym 79:59–67

16. Guo B, Chen F, Lei Y, Liu X, Wan J, Jia D (2009) Styrene-butadiene rubber/halloysite nanotubes nanocomposites modified by sorbic acid. Appl Surf Sci 255:7329–7336

17. Tian M, Qu C, Feng Y, Zhang L (2003) Structure and properties of fibrillar silicate / SBR composites by direct blend process. J Mater Sci 8:4917–4924

18. Ramesan MT, Anilkumar T (2009) Preparation and properties of different functional group containing styrene butadiene rubber. J Chil Chem Soc 54:23–27

19. Elizabeth KI, Alex R, Kuriakose B, Varghese S, Peethambaran NR (2006) Dichlorocarbene modification of natural rubber and its role as a modifier in blends of natural rubber and hydrogenated nitrile rubber. J Appl Polym Sci 101:4401–4409

20. Ramesan MT, Alex R (2000) Dichlorocarbene modified SBR - vulcanization behaviour and physical properties. Kautsch Gummi Kunstst 53:596–600

21. Ramesan MT, Nihmath A, Francis J (2013) Preparation and characterization of zinc sulphide nanocomposites based on acrylonitrile butadiene rubber. AIP Conf Proc 1536:255–257

22. Ramesan MT, Alex R (1998) Dichlorocarbene modification of styrene – butadiene rubber. 68: 153–160

23. Pich A, Hain J, Prots Y, Adler HJ (2005) Composite polymeric particles with ZnS shells. Polymer 46:7931–7944

24. Jasna VC, K. Priyanka K, Mathew G, Ramesan MT (2018) Evaluation of spectral, thermal, flame retardant, dielectric, solvent diffusion and transport behavior of novel nanocomposite derived from chlorinated styrene butadiene rubber and nanganous tungstate. Polym Compos. https://doi.org/10.1002/pc.24846

25. Ramesan MT, Santhi V, Bahuleyan BK, Al-Maghrabi MA (2018) Structural characterization, material properties and sensor application study of in situ polymerized polypyrrole/silver doped titanium dioxide nanocomposites. Mater Chem Phys 211:343–354

26. Al-Kadhemy MFH, Hussein R, Al-Zuky AAD (2012) Analysis of the absorption spectra of styrene-butadiene in toluene. J Phys Sci 23:89–100

27. Zhang Y, Lu F, Wang Z, Wang H, Kong M, Zhu X, Zhang L (2007) ZnS nanoparticle-assisted synthesis and optical properties of ZnS nanotowers. Cryst Growth Des 7:1459–1462

28. Noriman NZ, Ismail H (2012) Effect of epoxidized natural rubber on thermal properties, fatigue life, and natural weathering test of styrene butadiene rubber/recycled acrylonitrile-butadiene rubber (SBR/NBR) blends. J Appl Polym Sci 123:779–787

29. Ramesan MT, Jose C, Jayakrishnana P, Anilkumar T (2018) Multifunctional ternary composites of poly (vinyl alcohol)/cashew tree gum/pumice particles. Polym Compos 39:38–45

30. Laoutid F, .Bonnaud L, Alexandre M, Cuesta JML, Dubois Ph (2009) New prospects in flame retardant polymer materials: from fundamentals to nanocomposites. Mater Sci Eng R Rep 63: 100–125

31. Ramesan MT (2014) Flammability, oil resistance and interaction of petroleum fuels with dichlorocarbene modified styrene butadiene rubber/fly ash composites. Pet Sci Technol 3:1775–1783

32. Jayakrishnan P, Ramesan MT (2017) Synthesis, characterization, electrical conductivity and material properties of magnetite/polyindole/poly(vinyl alcohol) blend nanocomposites. J Inorg Organomet Polym Mater 27:323–333

33. George SC, Knörgen M, Thomas S (1999) Effect of nature and extent of crosslinking on swelling and mechanical behavior of styrene-butadiene rubber membranes. J Membr Sci 163:1–17

34. Ramesan MT (2014) Effect of fly ash on thermal sability, flammability, oil resistance and transport properties of chlorinated styrene butadiene rubber composites. J Elastomers Plast 46:303–324

35. Sujith A, Unnikrishanan G (2005) Barrier properties of natural rubber/ethylene vinyl acetate/carbon black composites. J Mater Sci 40:4625–4640

36. Sareena C, Ramesan MT, Purushothaman E (2013) Transport studies of peanut shell powder reinforced natural rubber composites in chlorinated solvents. Fibers Polym 14:1674–1687

37. Ramesan MT (2015) Effects of magnetite nanoparticles on morphology, processability, diffusion and transport behavior of ethylene vinyl acetate nanocomposites. Int J Plast Technol 19:368–380

38. Ramesan MT (2015) Poly (ethylene-co-vinyl acetate)/ magnetite nanocomposites: interaction of some liquid fuels, thermal and oil resistance studies. Polym Polym Compos 23:85–92

39. Padhi S, Achary PGR, Nayak NC (2015) Molecular transport behaviour of organic solvents through halloysite nanotubes filled ethylene-vinyl acetate copolymer. Bull Mater Sci 38:925–933

40. Sareena C, Sreejith MP, Ramesan MT, Purushothaman E (2015) Transport properties of coconut shell powder (CSP)-reinforced natural rubber composites in aromatic solvents. Polym Bull 72: 1683–1702

41. Saatchi MM, Shojaei A (2012) Effect of carbon-based nanoparticles on the cure characteristics and network structure of styrene-butadiene rubber vulcanizate. Polym Int 61:664–672

42. Balachandran M, Bhagawan SS (2012) Mechanical, thermal and transport properties of nitrile rubber (NBR)-Nanoclay composites. J Polym Res 19:9809